Marine Chemistry xxx (xxxx) xxx–xxx

Contents lists available at ScienceDirect

Marine Chemistry

journal homepage: www.elsevier.com/locate/marchem

The important role of submarine groundwater discharge (SGD) to derive nutrient fluxes into River dominated Ocean Margins – The East China Sea

Xilong Wang[a,b], Mark Baskaran[c], Kaijun Su[a,d], Jinzhou Du[a,*]

[a] State Key Laboratory of Estuarine and Coastal Research, East China Normal University, Shanghai 200062, PR China
[b] Guangxi Key Laboratory of Marine Disaster in the Beibu Gulf, Qinzhou University, Qinzhou 535011, PR China
[c] Department of Geology, Wayne State University, Detroit, MI 48202, USA
[d] Institute of Radiation Medicine, Chinese Academy of Medical Sciences and Peking Union Medical College, Tianjin 300192, PR China

ARTICLE INFO

Keywords:
East China Sea (ECS)
Radium isotopes
Submarine groundwater discharge (SGD)
Nutrient fluxes

ABSTRACT

Submarine groundwater discharge (SGD), which has been recognized as an important pathway for the transport of terrestrial chemical components (i.e., nutrients, trace elements and other contaminants) to the ocean, plays an important role on the biogeochemical cycling in marine environment, especially coastal/marginal seas. In the present work, the initial results on the amount of SGD into the continental shelf of the East China Sea (ECS), one of the marginal seas with large riverine input from the Changjiang River (Yangtze River) are evaluated. According to the locations and features of water masses in the ECS, radium (Ra) isotopes mass balance model was built and the conservative and non-conservative (excess) components of Ra were evaluated. Using the inventories of excess ^{228}Ra and ^{226}Ra, the residence time of water in the ECS was estimated as 1.30 ± 0.27 years. Then the SGD flux was estimated to be (5.42 ± 0.14) × 10^{11} m^3 yr^{-1}, which were 47 ± 1% of the total river discharge into the ECS along the coast. Nutrient fluxes driven by SGD were estimated to be (7.32 ± 0.19) × 10^{10}, (1.79 ± 0.05) × 10^9 and (1.59 ± 0.04) × 10^{11} mol yr^{-1} for dissolved inorganic nitrogen (DIN), dissolved inorganic phosphorus (DIP) and dissolved inorganic silicate (DSi), respectively, which were about 0.7, 2.2 and 1.4 times, respectively, of the riverine inputs. Furthermore, SGD-driven nutrient had obviously high DIN/DIP ratios, which could lead to a number of large-scale environmental problems to the ECS, such as the frequent harmful algal blooms and hypoxia especially in the estuary and coastal area.

1. Introduction

River dominated Ocean Margins (RiOMars) receive various weathering products and pollutants in both dissolved and particulate forms from riverine input. Therefore, the RiOMars are the major depocenter of not only terrestrial sediments but also biogenic elements and organic matter (Aller, 1998; Bianchi and Allison, 2009; Burdige, 2007; Hedges and Keil, 1995; Meade, 1996; McKee et al., 2004; Nozaki et al., 1991). Recently, studies have been attempted to quantify the fluxes and cycling of materials to the RiOMars. For example, the transformation of dissolved and particulate materials on continental shelves influenced by the Mississippi River has been reported (Bianchi and Allison, 2009). This system delivered substantial amounts of inorganic nutrient, including nitrogen (N), phosphorus (P) and silica (Si) to coastal environments. However, in addition to the riverine input, the amount of chemical materials (e.g. biogenic elements) delivered into such RiOMars (i.e. the Gulf of Mexico) via submarine groundwater discharge (SGD) could also be comparable to that by riverine input (Santos et al., 2008, 2009). In the northeastern coastal Gulf of Mexico, it was shown that the riverine water inputs was comparable to the amount of SGD estimate (Santos et al., 2008). The SGD-derived N and dissolved organic carbon (DOC) fluxes were comparable to that from the main regional rivers (Santos et al., 2008). Although they did not make a comparison to the Mississippi River, one could see that SGD plays a major role in the biogeochemical processes in the subterranean estuary of the Gulf of Mexico. As one of the typical RiOMars, the East China Sea (ECS) receives various substances (pollutants and other materials) in both dissolved and particulate forms from the world's third largest river-Changjiang River (Yangtze River). Thus, it is of great interest to quantify the amount of SGD-derived nutrient into the ECS.

The ECS is one of the largest marginal seas in the world with an area of approximately 0.7 × 10^6 km^2, having a vast continental shelf and is bordered by the Okinawa Trough with a maximum depth exceeding 2000 m. It is also one of the most productive areas of the world's oceans. The Changjiang River disperses over the ECS forming a buoyant plume called the Changjiang effluent plume (CEP) and empties into the ECS

* Corresponding author.
E-mail address: jzdu@sklec.ecnu.edu.cn (J. Du).

https://doi.org/10.1016/j.marchem.2018.05.010
Received 20 February 2018; Received in revised form 2 May 2018; Accepted 31 May 2018

shelf with large nutrient inputs (Chen, 1996). In the previous work, it was reported that the flux of SGD into the Changjiang River effluent plume (CEP) was estimated to be (0.2–1.0) × 10^9 m^3 d^{-1} which is equivalent to 6–30% of the Changjiang River water discharge during flood season (Gu et al., 2012). In addition, it was shown that the SGD may be another important nutrient source to the ECS, although there is so large riverine input containing nutrient from runoff in the watershed of Changjiang River. Note that the previous work was confined to the CEP in flood season; we extend the study regions in the present work to cover the major part of the continental shelf in the ECS.

Radium isotopes (^{226}Ra, ^{228}Ra, ^{223}Ra and ^{224}Ra, with half-lives 1602 years, 5.75 years, 11.4 days and 3.66 days, respectively) have been shown to be powerful tools to assess the sources and quantify SGD fluxes to coastal waters. Although a few earlier studies on bio-elements budgets or mass balance have been made in the ECS, quantifications of the impacts of the SGD on material budgets or mass balance to this region has not been reported. Therefore, our aim is to quantify the SGD fluxes and thereby nutrient using these natural radium isotopes. Such information is anticipated to promote our understanding of not only biogeochemical recycling processes but also eco-environment processes (i.e. hypoxia, red tidal etc.) in the ECS.

2. Sampling and analysis

2.1. Study site

The ECS is one of the largest marginal seas in the world. The major part of the ECS is the continental shelf zone which is shallower than 200 m depth. This continental shelf is influenced by multiple water masses: Changjiang Diluted Water (CDW), Taiwan Warm Current (TWCW), Yellow Sea Cold Water (YSCW, only in summer) and Kuroshio Water Current (KSW) offshore (Beardsley et al., 1985; Lee and Chao, 2003). Details on the current systems can be found in Yuan and Hsueh (2010).

The Changjiang River, one of the largest rivers in the world, empties into the ECS shelf with large amounts of nutrient input (Chen, 1996), making the coastal waters of the ECS a highly productive water. The impact of the river in the form of Changjiang River plume varies seasonally and has an important effect on the distribution of water masses in the ECS. In summer, when the Changjiang floods, the plume spreads eastwards over the broad ECS, reaching as far as Cheju Island and the shelf-break. In the low discharge season, the Changjiang effluents are restricted to the western side of the ECS and move southward forming a narrow but turbid belt along the coast of China and reach the Taiwan Strait (Su, 1998).

2.2. Field sampling

Field sampling for this study was carried out in August 2013. The water depth varied from 9 to 1512 m from the nearshore to offshore, and the study area extended from the freshwater end of the Changjiang River to 127.00°E and from 25.50°N to 33.50°N. Fig. 1 shows the station locations in the ECS. At each station, temperature and salinity profiles were obtained using an in-situ SBE-25 SEALOGGER CTD (Conductivity-Temperature-Depth Sensor, Seabird Electronics). For radium analysis, large volume (60–100 L) water samples were collected using a submerged pump from 1 to 2 m depth below the surface and a large capacity (80 L) hydrophore from the water column at different depths. Groundwater and pore water samples (10 − 20 L) were also collected along the coast of the ECS, Shanghai-Zhejiang-Fujian province.

Based on the topography of Min-Zhe coastal waters overlaid with MODIS images of chlorophyll-*a*, Wu (2015) confirmed the presence of offshore penetrating fronts at specific locations in waters off the Min-Zhe coast which occur in response to buoyant coastal water along isobaths undulation of the ambient pycnocline. The chlorophyll-*a* data indicates the location of nutrient-rich coastal water influenced by the Changjiang River plume, thus the penetrating front plays an important role in cross-shelf material exchange in the ECS. The location of this penetrating front was along the 60 m isobaths which was found to be roughly parallel to the coast. In order to analyze the biogeochemical processes of Ra in the ECS, we divided the continental shelf into two parts based on this 60 m isobaths: the inner shelf (water depth shallow than 60 m) and the outer shelf (water depth deeper than 60 m).

2.3. Analysis of water samples

The sample collection, preconcentration and subsequent analysis of the collected water samples performed were outlined in our previous publications (Gu et al., 2012; Ji et al., 2013). Briefly, after filtering water with pre-filter cartridges (pore size: 0.5 μm), Ra isotopes in the dissolved water were extracted using a MnO_2-impregnated acrylic fiber column (20 g) with an approximately 0.5 L·min^{-1} flow rate. Then the activities of ^{223}Ra and ^{224}Ra were measured using the Radium Delayed Coincidence Counter system (RaDeCC) (Moore and Arnold, 1996). All of the water samples were also analyzed for ^{228}Th to determine parent-supported ^{224}Ra and this parent-supported ^{224}Ra was utilized in the determination of excess ^{224}Ra (excess ^{224}Ra = measured ^{224}Ra - ^{228}Th activity). The activities of long-lived isotopes, ^{226}Ra and ^{228}Ra, were measured by HPGe-gamma-ray spectrometry (Wang et al., 2014). The groundwater and pore-water samples (60 mL) for nutrient analysis were collected and stored following the procedure given in published literature (Su et al., 2011; Ji et al., 2013). The nutrient samples were analyzed using an auto-analyzer (Model: Skalar SANplus146) (Liu et al., 2005). The concentration of total dissolved inorganic nitrogen (DIN) reported in this article is the sum of NO_2^-, NO_3^- and NH_4^+.

3. Results

3.1. Hydrographic characteristics

The surface water temperature in the continental shelf of the ECS during August 2013 cruise ranged from 23.1 °C (Station B1) to 30.9 °C (Station O3) and salinity varied from 0.2 (Stations O7 and O8, fresh water end-member) to 35.5 (Station A8). The temperature of the near bottom water ranged from 9.0 °C (Station F8) to 30.7 °C (Station O3) and the salinity varied from 0.1 (the same surface water station) to 34.7 (Station E6). Fig. 2 shows the horizontal distributions of temperature and salinity in the surface and near bottom water of the ECS in August 2013. As expected, the salinity shows an increasing trend from coastal to shelf/slope waters not only in the surface water but also in the near bottom water. A clear discernable signal of the CDW (low salinity) in the northwest of the study region, with salinities lower than 31, can be observed; the influence of the CDW extends to 126.00°E, and such a distribution is consistent with the results published earlier (Chang and Isobe, 2003; Wu et al., 2011, 2014). However, the contour line of the salinity value of 34 was closer in bottom water than the surface water near the coastal area, which indicates that the surface water can be influenced more easily than the near bottom water by the CDW. The YSCW signature was found in the northwest of the study area resulting in lower temperature. The KSW and the TWCW with higher temperature and salinity flow along the slope and the mid continental shelf. Therefore, the observed distribution of the temperature and salinity is primarily due to the impact of the CDW (low salinity), KSW (high temperature and high salinity), TWCW (high temperature and high salinity) and YSCW (low temperature in summer) currents.

3.2. The activities of Ra isotopes in the ECS

The activities of dissolved ^{224}Ra, ^{223}Ra, ^{226}Ra and ^{228}Ra in the continental shelf water of the ECS ranged from below detection limit to 200 dpm 100 L^{-1} (geometric mean: 4.2 ± 3.4 dpm 100 L^{-1}, n = 159), below detection limit to 8.23 dpm 100 L^{-1} (geometric mean:

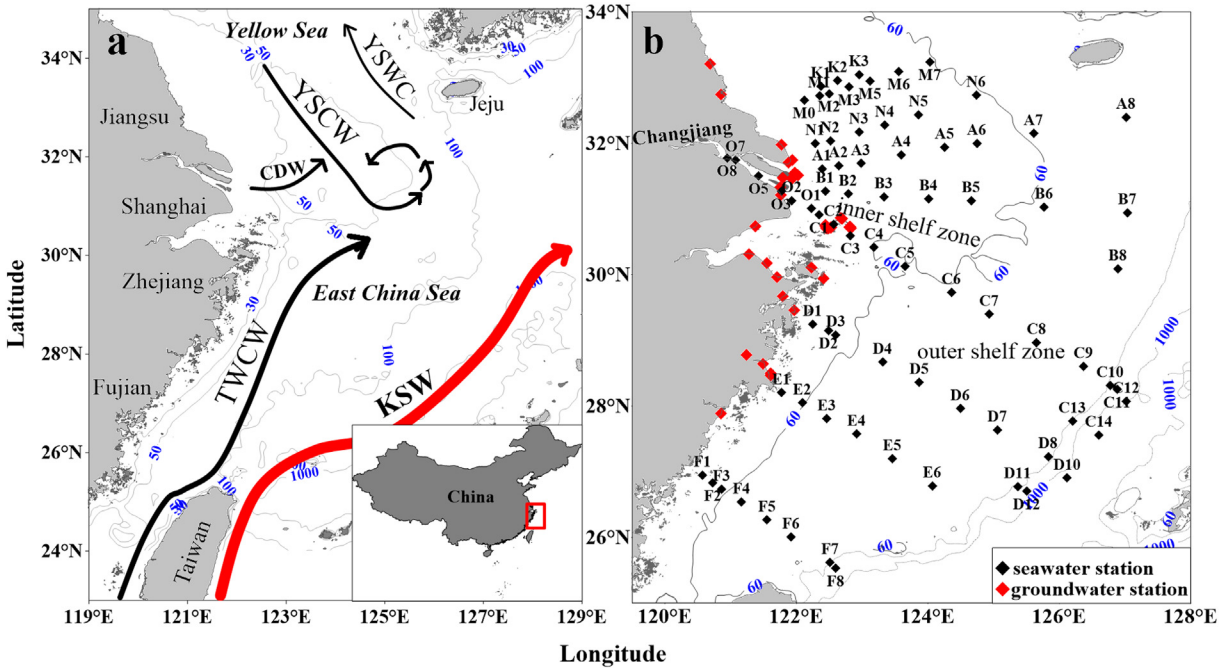

Fig. 1. The location of the study area (a) and Sampling locations (b) in this study including seawater sample stations in the ECS and groundwater sample stations along the coast of the ECS. The black diamonds are the seawater sampling sites, and the red diamonds are the groundwater sampling sites. The 60 m isobaths shown in the map separated the inner shelf and outer shelf according to the cross-shelf penetrating fronts reported by Wu (2015). (a) The chart of currents in summer in the ECS modified after Su (1998): Changjiang Dilute water (CDW); Yellow Sea Cold Water (YSCW); Yellow Sea Warm Current (YSWC); Taiwan Warm Current Water (TWCW); Kuroshio Current Water (KSW). (For interpretation of the references to colour in this figure legend, the reader is referred to the web version of this article.)

0.7 ± 0.7 dpm 100 L^{-1}, n = 159), 6.92 to 36.6 dpm 100 L^{-1} (geometric mean: 12.5 ± 6.6 dpm 100 L^{-1}, n = 119), and 0.39 to 105 dpm 100 L^{-1} (geometric mean: 21.8 ± 10.0 dpm 100 L^{-1}, n = 119), respectively (note that in the calculation of mean, the below detection limit is taken as zero; since the range varies over two orders of magnitude, the geometric mean is given). Except for the high values at the Changjiang estuary, the activities of the radium isotopes (^{226}Ra and ^{228}Ra) fall generally within the range summarized for the global ocean surface water (Cochran, 1992). However, there are some very high activities of ^{228}Ra (72–105 dpm 100 L^{-1}, n = 8) and ^{224}Ra (70–200 dpm 100 L^{-1}, n = 6) reported within 100 km from the coast (water depth < 36 m). Fig. 3 shows the horizontal distributions of the four Ra isotopes in the surface water and near bottom water of the ECS. For the short-lived ^{224}Ra and ^{223}Ra, the high levels appear to be near the shoreline. The activities of ^{224}Ra is below the detection limit outside the 50 m isobaths in the northern region of the ECS; however, in the south, the ^{224}Ra activities sharply decrease with distance. The distribution of ^{223}Ra is generally similar to that of ^{224}Ra. Although the activities of ^{223}Ra are low, it can be found up to 300 km far from the land north of Changjiang River mouth, and its activity decreased drastically offshore. For the long-lived Ra, their activities exhibited significant spatial variability in the study area. The maximum activities of ^{226}Ra in the surface water occurred at the north of the Changjiang River Estuary near the Yellow Sea in summer. Lower activities were found in the southeast side of the ECS. There are similarities in the distribution of ^{228}Ra and ^{226}Ra, with the high activities of ^{228}Ra in the surface water along the Zhejiang coast and Jiangsu coast and a decreasing trend from the nearshore to the offshore.

Compared to the surface water in the shelf and slope waters of ECS, the distribution of Ra in the near bottom water showed a clearly contrasting trend. The signal of short-lived ^{224}Ra and ^{223}Ra in the coastal area could be detected even in the outer shelf, near middle of the ECS. The location of the contour line in the near bottom water was observed to be farther away from the land in contrast to that in the surface water. In addition, the average activity of ^{224}Ra and ^{223}Ra at the bottom water was slightly higher than that in the surface water, which could be due to the influence from thorium (Th, the parent of Ra) in the bottom sediment. The signal of long-lived ^{226}Ra and ^{228}Ra exhibited a totally different distribution trend compared to that of the short-lived ^{223}Ra and ^{224}Ra. Comparing the contour line for ^{226}Ra and ^{228}Ra activities in the near bottom water to that in the surface water, the location of contour line was closer to the coastal area than farther offshore. This is attributed to high Ra in the coastal water from the diffusional input from bottom sediment as well as SGD input (Moore, 1996; Krest et al., 1999; Gu et al., 2012; Gu, 2015). Gu et al. (2012) have reported that SGD was the main source of high Ra in the Changjiang effluent plume which accounted for ~49% of the total input. Therefore, it is predicted that higher Ra activities in coastal waters originate from terrigenous inputs via SGD input in this study. In addition, the distribution of long-lived Ra demonstrates the mixing of offshore seawater (low Ra) with nearshore freshwater (high Ra).

^{226}Ra and ^{228}Ra activities in the groundwater samples collected along the coastal region in the ECS are given in Table 1, including the data from Chongming and Shengsi Islands published by Gu et al. (2012). Most of the ^{226}Ra activities in wells along Zhejiang and Shanghai under the current investigation ranged between 6.93 and 59.9 dpm 100 L^{-1}, but in four groundwater samples the activities were higher than 90 dpm 100 L^{-1}, from 90.5 to 140 dpm 100 L^{-1}. In contrast, the ^{228}Ra activities in most of the groundwater samples ranged from 10.3 to 157 dpm 100 L^{-1}, with four samples having much higher activities, from 239 to 458 dpm 100 L^{-1}. These four values are higher than the highest value in Chongming Island (157 dpm 100 L^{-1}) and Shengsi Island (108 dpm 100 L^{-1}, Gu et al., 2012). A set of three samples with very high ^{228}Ra/^{226}Ra activity ratios of 4.3 to 5.1 (n = 3) were found in the groundwater samples which are significantly higher compared to values from Chongming and Shengsi groundwater samples (Gu et al., 2012).

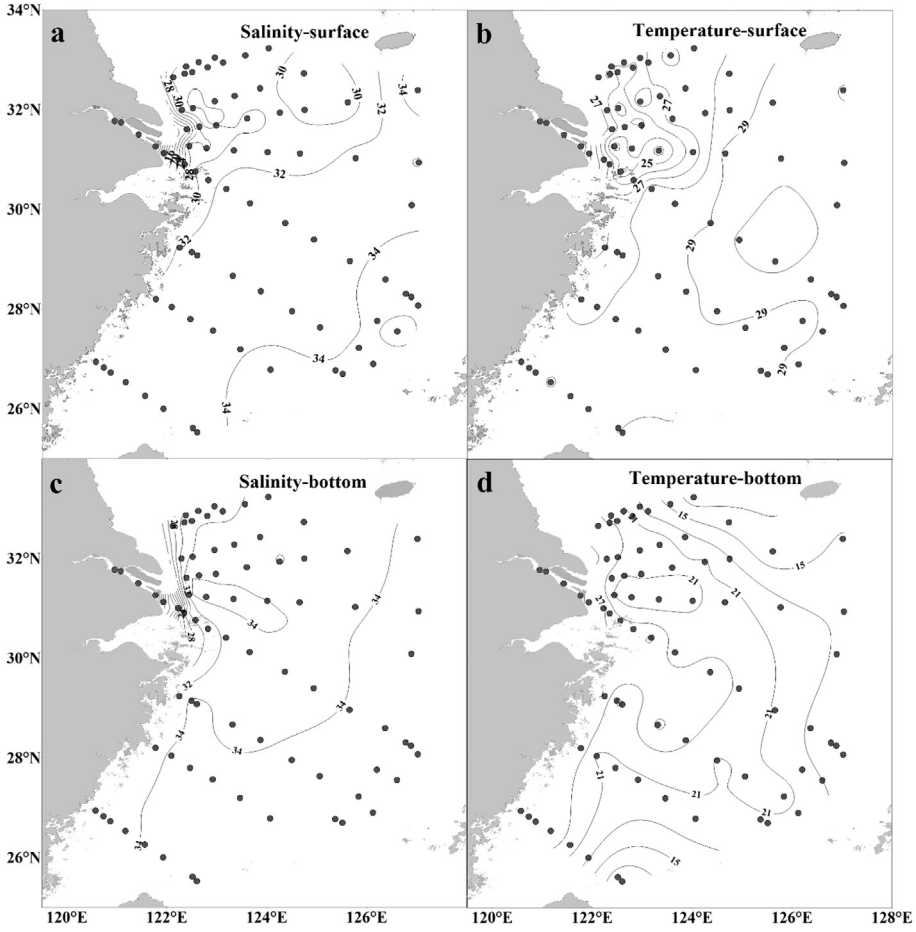

Fig. 2. The horizontal distributions of salinity (Psu) and temperature (°C) in the surface and bottom water of the ECS in August 2013. (a) Surface salinity, (b) Surface temperature, (c) Bottom salinity, (d) Bottom temperature.

3.3. Concentration of nutrient along the coastal region in the ECS

The average concentrations of nutrient (in μmol L^{-1}) in the groundwater, Changjiang River water and the surface water of ECS are listed in Table 2. The average concentrations (μmol L^{-1}) of DIN, PO_4^{3-} and SiO_3 in groundwater samples collected along the coast are 135 ± 79.5, 3.30 ± 1.98, and 293 ± 73.7 (n = 23), respectively (here the average concentration is the geometric mean), which were much higher (DIN: 1.8 and 4.1 times; PO_4^{3-}: 5.2 and 5.8 times; and SiO_3: 2.9 and 7.6 times) than the average value of the fresh water in the Changjiang River (75.1, 0.64 and 100 μmol L^{-1}) and surface water of the ECS, 32.3, 0.57 and 38.7 μmol L^{-1}, respectively in summer (Zhang et al., 2007a; Liu et al., 2009). Such high concentrations of these biogenic elements in groundwater may have a great influence on the biogeochemical cycling of the ECS eco-system from the SGD along the coastal region in the ECS.

4. Discussion

4.1. Ra sources

The activities of ^{224}Ra, ^{223}Ra, ^{226}Ra, and ^{228}Ra activities versus salinity in the surface water samples collected in the cruise are given in Fig. 4. Activities of all Ra isotopes had low values (^{224}Ra, ^{223}Ra, ^{226}Ra and ^{228}Ra: 12.1, 0.1, 13.0 and 14.03 dpm 100 L^{-1}) when the salinity was near zero. It's reported that dissolved ^{226}Ra and ^{228}Ra concentrations in Chanjiang River system in flood season were between 1.2 and 4.2 dpm 100 L^{-1}, 9.36 and 20.16 dpm 100 L^{-1} (Su et al., 2015) at the freshwater end (salinity~0) and then reached a maximum in the region with the salinity between 10 and 17. The activities of ^{228}Ra decreased at salinities > 17. Although there is a large scatter of the ^{223}Ra and ^{228}Ra activities between the salinity of 30 and 33, radium does not exhibit conservative behavior from the freshwater end to the seawater. It has been shown that radium is released from river-borne particulate matter at low salinity values with a lower K_d of Ra in seawater (Webster et al., 1995; Krest and Harvey, 2003; Gonneea et al., 2008). Thus, we separated Ra in surface water into conservative and non-conservative fractions. We assume the conservative fraction of Ra was contributed by the mixing processes occurring in the study area. The non-conservative fraction of Ra was mainly derived from desorption of the suspended particles, diffusion from bottom sediments and SGD.

4.1.1. Water masses with Ra mixing in the ECS

The continental shelf of the ECS is influenced by multiple water masses in summer (Fig. 1a): CDW, YSCW, TWCW and KSW offshore (Beardsley et al., 1985; Lee and Chao, 2003). The warm and salty KSW flows northward along the ECS shelf break and eventually develops into a branch, TWCW, which flows to the north in the middle region of the continental shelf (Feng et al., 1999). Therefore, the relative fractions of the three water masses (CDW, YSCW and TWCW) mentioned above in the ECS can be evaluated by the classical T-S property plot (Mao et al., 1964; Chen et al., 1995; Zeng et al., 2012).

Assuming that temperature and salinity are conservative in this study (implies surface heat exchange, evaporation, and precipitation are ignored), the fractions of three water masses can be estimated by Eq. (1) (Zhang et al., 2007b; Gu et al., 2012).

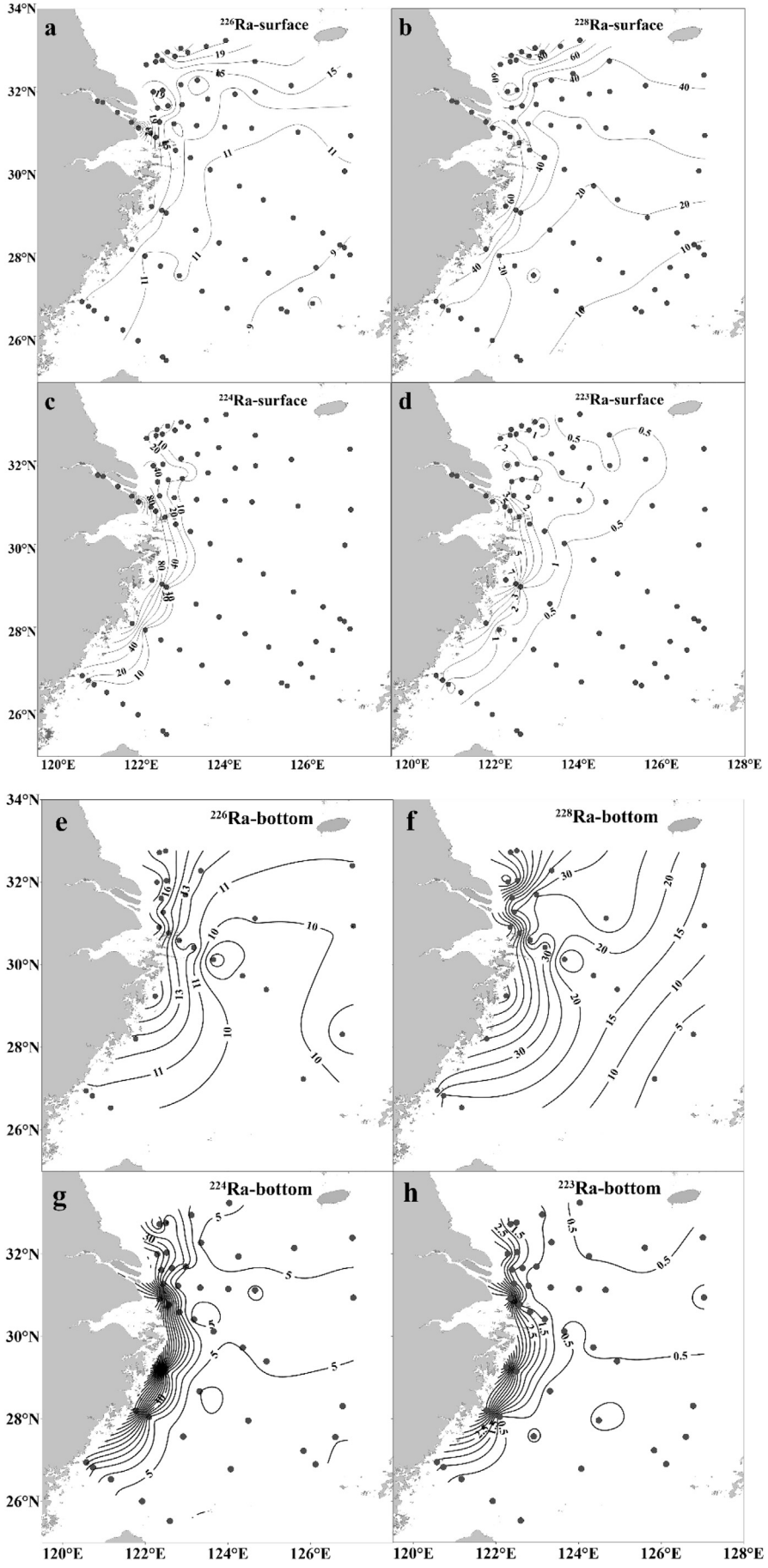

(caption on next page)

Fig. 3. The horizontal activities (dpm 100 L^{-1}) distributions of ^{226}Ra (a), ^{228}Ra (b), ^{224}Ra (c) and ^{223}Ra (d) in the surface water and ^{226}Ra (e), ^{228}Ra (f), ^{224}Ra (g) and ^{223}Ra (h) in the bottom water of the study area.

$$\begin{pmatrix} f_{YSCW} \\ f_{CDW} \\ f_{TWCW} \end{pmatrix} = \begin{pmatrix} 1 & 1 & 1 \\ T_{YSCW} & T_{CDW} & T_{TWCW} \\ S_{YSCW} & S_{CDW} & S_{TWCW} \end{pmatrix}^{-1} \begin{pmatrix} 1 \\ T_{obs} \\ S_{obs} \end{pmatrix} \quad (1)$$

where f_{YSCW}, f_{CDW}, and f_{TWCW} are the fractions of water derived from YSCW, CDW and TWCW, respectively; T_{YSCW} and S_{YSCW} are the temperature and salinity, respectively of the end-members of YSCW; T_{CDW} and S_{CDW} are the temperature and salinity, respectively of the end-members of CDW; T_{TWCW} and S_{TWCW} are the temperature and salinity, respectively of the end-members of TWCW; and T_{obs} and S_{obs} are the measured temperature and salinity, respectively at the stations in the study area.

To identify the fractional contribution from each of the three water masses, a knowledge of the end-members with the hydrographic parameters are required. In general, the hydrographic parameters were obtained by qualitative and quantitative analysis (e.g. clustering analysis) (Takano, 1991). The end member values of T and S in those three water bodies are listed in Table 3. The hydrographic data for all three major currents were obtained within the study area. The calculated mixing fractions of the three water masses in the ECS are shown in Fig. 5. The contributions of each water masses decreased with the increasing distance from their source region. Our calculations indicate that the average contributions of the three water masses (CDW, YSCW and TWCW) were 17%, 34% and 49%, respectively.

Since radium is a water tracer in seawater, when the water masses mix in the study area, radium from different water masses will also mix conservatively, similar to salinity and temperature. The expected activities of ^{223}Ra, ^{226}Ra and ^{228}Ra resulting from the mixing of three water masses in the study area could be calculated from the following equations:

$$^{223}Ra_{mix} = f_{CDW} \times {}^{223}Ra_{CDW} + f_{YSCW} \times {}^{223}Ra_{YSCW} + f_{TWCW} \times {}^{223}Ra_{TWCW} \quad (2)$$

$$^{226}Ra_{mix} = f_{CDW} \times {}^{226}Ra_{CDW} + f_{YSCW} \times {}^{226}Ra_{YSCW} + f_{TWCW} \times {}^{226}Ra_{TWCW} \quad (3)$$

$$^{228}Ra_{mix} = f_{CDW} \times {}^{228}Ra_{CDW} + f_{YSCW} \times {}^{228}Ra_{YSCW} + f_{TWCW} \times {}^{228}Ra_{TWCW} \quad (4)$$

where: $^{223}Ra_{mix}$, $^{226}Ra_{mix}$ and $^{228}Ra_{mix}$ are activities resulting from mixing of the three water masses at each station; $^{223}Ra_{CDW}$, $^{226}Ra_{CDW}$ and $^{228}Ra_{CDW}$ are ^{223}Ra, ^{226}Ra and ^{228}Ra end-members respectively in CDW; $^{223}Ra_{YSCW}$, $^{226}Ra_{YSCW}$ and $^{228}Ra_{YSCW}$ are ^{223}Ra, ^{226}Ra and ^{228}Ra end-members respectively in YSCW; $^{223}Ra_{TWCW}$, $^{226}Ra_{TWCW}$ and $^{228}Ra_{TWCW}$ are ^{223}Ra, ^{226}Ra and ^{228}Ra end-members in the TWCW. Here, due to the short-life and the sharply decreasing ^{224}Ra activity with distance from land, we did not use ^{224}Ra in the three endmembers

Table 1
The locations and activities of ^{226}Ra and ^{228}Ra in groundwater samples collected along the coast of ECS.

Station	Longitude (°E)	Latitude (°N)	Salinity	^{226}Ra	Error	^{228}Ra	Error	^{228}Ra/^{226}Ra
			(Psu)	(dpm 100 L^{-1})				
GW	120.848	27.882	2.3	14.9	1.2	33.8	3.4	2.3
	122.228	30.102	0.2	24.8	1.4	32.2	3.4	1.3
	122.412	29.938	0.6	36.1	1.6	105.6	4.6	2.9
	121.493	28.644	14.6	139.7	2.5	378.5	7.9	2.7
	121.241	28.777	2.1	17.6	1.4	30.3	3.6	1.7
	121.607	28.47	–	52.1	3.4	239.0	9.7	4.6
	121.551	30.171	–	40.4	1.2	92.1	3.4	2.3
	121.275	30.314	6.7	59.9	1.6	258.3	5.0	4.3
	121.371	30.733	9.3	90.5	2.3	458.1	8.3	5.1
	121.763	31.211	0.7	11.7	0.8	27.0	2.7	2.3
	121.787	31.474	0.5	9.3	1.3	18.3	3.0	2.0
	121.772	31.855	8.5	75.2	2.5	234.0	8.5	3.1
	121.848	31.977	8.9	60.6	2.5	242.0	11.4	4.0
	121.245	31.869	0.8	24.3	1.5	45.4	5.0	1.9
	121.772	31.976	6.67	37.9	2.0	110.0	4.6	2.9
	120.752	33.268	6.9	26.3	2.1	55.3	4.2	2.1
	121.934	31.746	16.6	55.1	2.3	241.0	5.1	4.4
Chongming Island (Gu et al., 2012)	121.94	31.46	1.9	16.9	0.8	26.5	1.2	1.6
	121.93	31.46	0.7	7.5	0.4	11.0	0.4	1.5
	122.02	31.51	12.5	56.9	1.9	96.1	3.4	1.7
	121.98	31.51	11.8	47.3	3.8	62.2	4.3	1.3
	121.98	31.55	7.9	47.1	1.7			
	121.97	31.54	10	48.5	2.0	156.7	6.1	3.2
Shengsi Islands (Gu et al., 2012)	122.48	30.71	0.1	13.3	1.4	42.8	2.4	3.2
	122.53	30.72	0.2	16.0	0.2	18.3	0.5	1.1
	122.52	30.72	0.2	6.9	0.3	11.2	0.5	1.6
	122.49	30.71	0.2	15.2	1.0	10.3	0.7	0.7
	122.45	30.71	0.2	16.6	0.9	52.7	3.0	3.2
	122.45	30.73	0.5	26.7	1.1			
	122.44	30.74	0.4	19.1	0.5			
	122.83	30.71	0.3	11.6	0.4	21.8	1.2	1.9
	122.82	30.73	0.1	9.0	0.8	20.9	0.9	2.3
	122.81	30.72	0.6	29.4	0.6	73.8	5.1	2.5
	122.81	30.73	0.5	121.4	6.9	107.8	18.2	0.9
	122.69	30.85	0.7	45.1	1.0			
	122.67	30.86	0.2	129.9	6.5			
	122.69	30.85	0.4	16.0	0.2	18.3	0.5	1.1
Geomean				29.0	1.2	59.3	3.0	2.2

Table 2
The average concentrations of nutrients in groundwater, seawater and Changjiang fresh water end-members.

Watertype	DIN	DIP	DSi	DIN/DIP	DSi/DIN	Reference for nutrient
	μmol L^{-1}					
Groundwater	135 ± 79.5 n = 23	3.30 ± 1.98 n = 23	293 ± 73.7 n = 23	40 ± 49.8 n = 23	2.18 ± 1.05 n = 23	Geometric mean of the groundwater
Seawater	32.3	0.57	38.7	5–134	0.5–2.0	Zhang et al., 2007a; Liu et al., 2009
Changjiang	75.1	0.64	100	117	1.33	Wang et al., 2015

mixing equation. The radium end-member values are listed in Table 3.

4.1.2. Excess Ra in the ECS

From Eqs. (2), (3) and (4), the calculated Ra activities at each station in the study area were estimated and were found to be less than the measured Ra activities, which indicates additional input from other sources. This difference between the measured Ra and the calculated Ra-based three end-member mixing calculations is denoted as 'excess Ra (Ra_{ex})' in this article. This excess Ra is given as:

$$^{223}Ra_{ex} = {}^{223}Ra_{mea} - {}^{223}Ra_{mix} \quad (5)$$

$$^{226}Ra_{ex} = {}^{226}Ra_{mea} - {}^{226}Ra_{mix} \quad (6)$$

and

$$^{228}Ra_{ex} = {}^{228}Ra_{mea} - {}^{228}Ra_{mix} \quad (7)$$

where $^{223}Ra_{ex}$, $^{226}Ra_{ex}$ and $^{228}Ra_{ex}$ are excess ^{223}Ra, ^{226}Ra and ^{228}Ra activities and $^{223}Ra_{mea}$, $^{226}Ra_{mea}$ and $^{228}Ra_{mea}$ are measured activities at each station. In order to calculate the excess Ra inventory, an orthogonal horizontal linear grid was designed to map the ECS system with the spatial (area) scale of 1.11 km × 1.11 km. The excess Ra activities (Eqs. (5), (6) and (7)) and the depth of each station were then interpolated to the grid cells using the kriging method. Because the water column is not always well-mixed, we integrated the Ra for the whole water column. For stations nearshore, the average Ra between the surface and bottom water was used since these stations were too shallow to collect more than three samples. For stations offshore, the exponential fitting between radium and the depths was done at each station and the fitting line was integrated from the surface to the bottom. Then, excess Ra inventory (dpm m^{-2}) in the water whole water column for the inner and outer shelf were calculated as the sum of the integrated excess activity (dpm m^{-2}) in the water column multiplied by the area of each grid cell. The total excess inventory can be expressed by the following equations:

$$I^{223}Ra_{ex} = \sum_{i=1}^{n} \int_{H(i)}^{0} {}^{223}Ra_{ex}(i) \times S(i) \quad (8)$$

$$I^{226}Ra_{ex} = \sum_{i=1}^{n} \int_{H(i)}^{0} {}^{226}Ra_{ex}(i) \times S(i) \quad (9)$$

$$I^{228}Ra_{ex} = \sum_{i=1}^{n} \int_{H(i)}^{0} {}^{228}Ra_{ex}(i) \times S(i) \quad (10)$$

where $I^{223}Ra_{ex}$, $I^{226}Ra_{ex}$ and $I^{228}Ra_{ex}$ are the excess ^{226}Ra and ^{228}Ra inventories of the system, respectively; $\int_{H(i)}{}^{0}{}^{223}Ra_{ex}(i)$, $\int_{H(i)}{}^{0}{}^{226}Ra_{ex}(i)$ and $\int_{H(i)}{}^{0}{}^{228}Ra_{ex}(i)$ are the excess ^{223}Ra, ^{226}Ra and ^{228}Ra of the vertical water column in each grid cell (dpm m^{-2}), respectively; $H(i)$ is the average water depth of each grid cell; $S(i)$ is the area of each grid cell. Then the inventories of excess ^{223}Ra, ^{226}Ra and ^{228}Ra in the continental shelf of the ECS were estimated to be 3.42×10^{14}, 6.98×10^{14} and 3.95×10^{15} dpm, respectively, among which 5.95×10^{13}, 7.30×10^{13} and 4.53×10^{14} dpm of excess ^{223}Ra, ^{226}Ra and ^{228}Ra, respectively were in the inner shelf zone.

The distribution of excess Ra calculated using Eqs. (5), (6) and (7) is

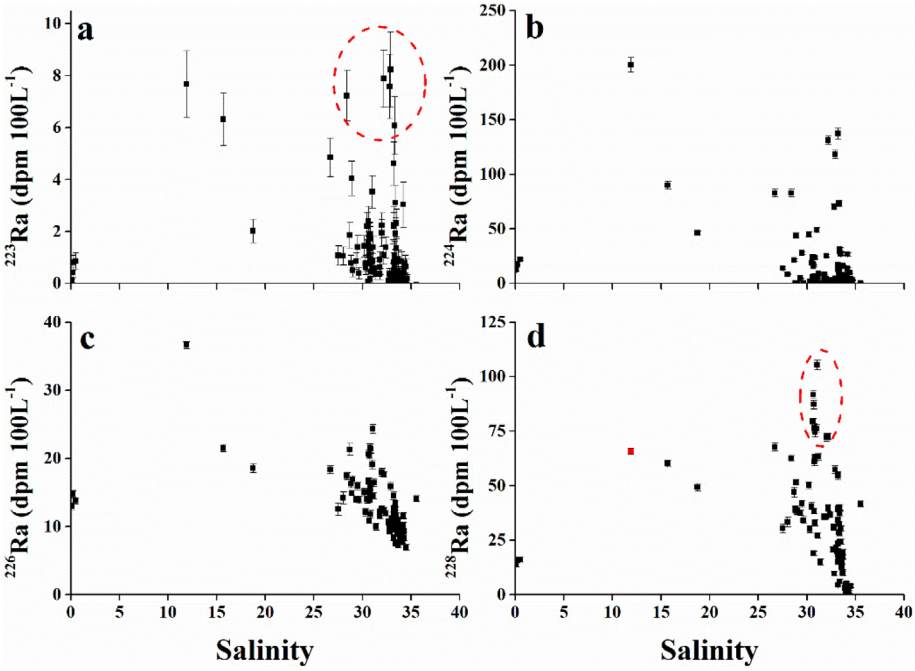

Fig. 4. Plots of Ra isotopes (^{223}Ra (a), ^{224}Ra (b), ^{226}Ra (c) and ^{228}Ra (d)) activities versus salinity for water samples collected in the ECS. The dash circles for ^{223}Ra and ^{228}Ra show the much scattered points between the salinity of 30 and 33.

Table 3
The temperature, salinity, ^{226}Ra, ^{228}Ra and ^{223}Ra end-member values of the three water masses, respectively.

Water	Temperature	Salinity	^{226}Ra	^{228}Ra	^{223}Ra	Reference	
Masses	℃	Psu	dpm 100 L^{-1}			For temperature and Ra	For salinity
CDW	28.1 ± 0.5	18.0 ± 3.0	21.5 ± 0.6	60.1 ± 1.6	0.86 ± 0.30	The estuary station O1	Zhang et al., 2007b and Feng et al., 1999
YSCW	21.7 ± 0.5	31.0 ± 0.4	11.6 ± 0.4	35.9 ± 1.1	0.62 ± 0.28	Nozaki et al., 1991	The average of the north N section
TWCW	30.3 ± 0.5	34.6 ± 0.4	7.57 ± 0.44	2.52 ± 0.94	0	Average of the most southern stations around 60 m isobaths	

shown in Fig. 6 which indicates that higher excess Ra near the coast. There are two possible sources for this excess Ra: diffusion from bottom sediments and SGD and the relative importance of these two terms are discussed below.

4.2. Residence time of the shelf waters in the ECS

It has been reported that the residence time of shelf waters could be estimated based on the mass balance of ^{226}Ra and ^{228}Ra (Nozaki et al., 1991). The ^{226}Ra–^{228}Ra pair is well suited due to the non-conservative mixing processes in the shelf area. For estimating the residence time of water in our study area, the mass balance approach of Ra was used. Assuming the system was in steady state, the relationship between excess Ra discussed above and the residence time could be expressed by:

$$^{226}Ra_{ex} = F_{226}\tau_w \tag{11}$$

$$^{228}Ra_{ex} = (F_{228} - \lambda_{228}{}^{228}Ra_{obs})\tau_w \tag{12}$$

$$^{223}Ra_{ex} = (F_{223} - \lambda_{223}{}^{223}Ra_{obs})\tau_w \tag{13}$$

where F_{223}, F_{226} and F_{228} are the total flux of ^{223}Ra, ^{226}Ra and ^{228}Ra due to the desorption from suspended particles, diffusive supply from bottom sediments and submarine groundwater discharge (dpm 100 L^{-1} yr^{-1}), respectively; τ_w is the mean residence time of water that receives excess Ra on the continental shelf; λ_{228} and λ_{223} are the decay constants of ^{228}Ra and ^{223}Ra, respectively. Since the decay of ^{226}Ra ($t_{1/2}$ = 1600 a) is negligible, eq. (11) is different from equations for ^{228}Ra and ^{223}Ra. Rearranging Eqs. (11), (12) and (13), we get:

$$\frac{^{228}Ra_{ex}}{^{226}Ra_{ex}} = \frac{F_{228}}{F_{226}} - \left(\frac{\lambda_{228}}{F_{226}}\right)^{228}Ra_{obs} \tag{14}$$

$$\frac{^{223}Ra_{ex}}{^{226}Ra_{ex}} = \frac{F_{223}}{F_{226}} - \left(\frac{\lambda_{223}}{F_{226}}\right)^{223}Ra_{obs} \tag{15}$$

The inventories of excess ^{226}Ra, ^{228}Ra and ^{223}Ra in the continental shelf discussed above were used to estimate the ratios of F_{228} and F_{226} as well as F_{223} and F_{226}. The estimated mean residence time of water in the continental shelf of the ECS is 1.30 ± 0.27 years, based on the Eqs. (11) and (14). In addition, the estimated mean residence time of the inner shelf water within the 60 m isobaths is 31.7 ± 14.6 days, based on Eqs. (11) and (15) (Table 4). These values can be compared to mean residence times in the ECS by earlier researchers: Nozaki et al. (1989): 2.3 ± 0.8 years for the shelf waters estimated by dividing the volume of shelf water (4.5×10^4 km^3) by the annual outflow of the shelf-derived water. This value was subsequently confirmed by Nozaki et al. (1991) based on excess ^{228}Ra/^{226}Ra activity ratio in the shelf water; Li (1995): 1 year, based on the box model of Kuroshio water flux of 22,000 ± 9000 km^3/a, and the volume of the shelf water of 2.2×10^4 km^3 (note that the residence time will be 2.1 years if volume of the shelf water is taken as 4.5×10^4 km^3); Yanagi (1994): 1.6 years based on the salt balance, with a Kuroshio water flux of 28,500 km^3/a; and Tsunogai et al. (1997): 0.8 ± 0.3 year, from the excess alkalinity mass balance. Thus, if appears that the mean residence time 1.30 ± 0.27 years for the whole continental shelf water of the ECS is reasonable.

4.3. The SGD estimation

As described above, the sources of radium to the water column include diffusive flux from the sediments, desorption from suspended particles, and SGD. Therefore, to estimate the SGD, a quantitative estimate of the diffusional flux and contribution from desorption is necessary. In the three end-member mixing model, we used for the end-member values (Table 3) of the CDW that also had included the desorption component from the riverine suspended particles (Fig. 4). Thus, the estimate from the desorption of the suspended particles was not considered separately.

4.3.1. Diffusive flux of radium through sediment in ECS shelf

It is widely known that long-lived radium isotopes in the oceanic water column are mostly derived from bottom sediments by diffusion. In shallow water environment, the maximum diffusive flux (FRa_{dif}) can be estimated from the equation given by Krest et al. (1999):

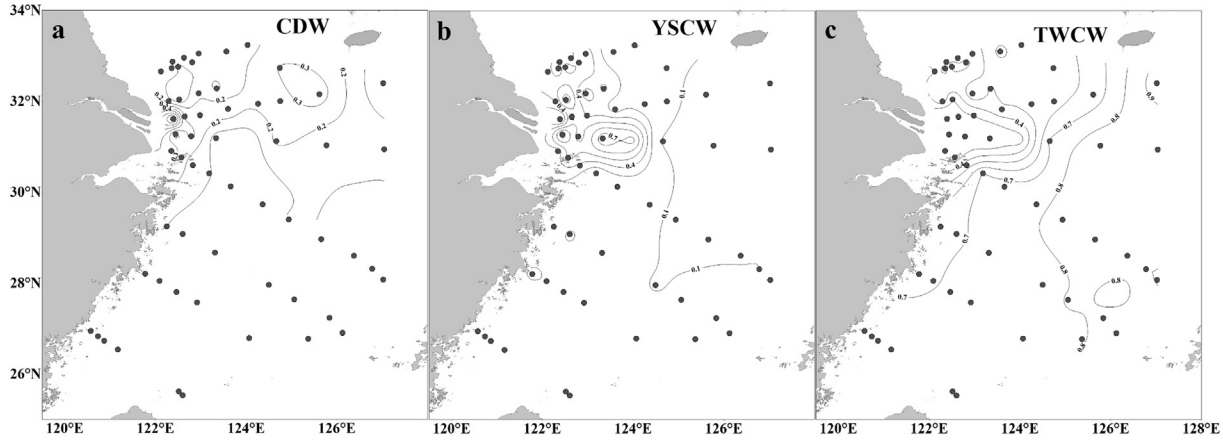

Fig. 5. The distributions of three water masses fractions in the ECS. (a) CDW, (b) YSCW, (c) TWCW.

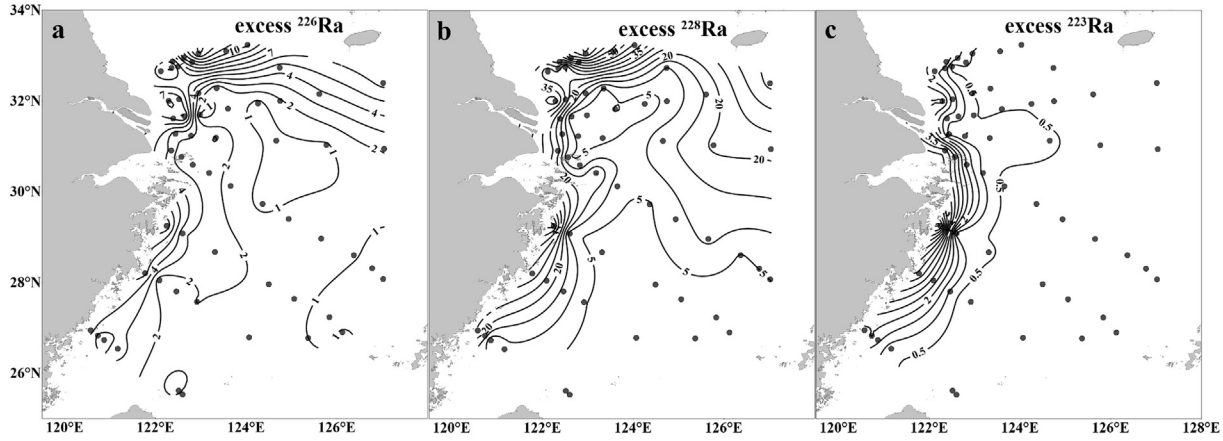

Fig. 6. The horizontal distributions of excess ^{226}Ra (a), ^{228}Ra (b) and ^{223}Ra (c) activities (dpm 100 L^{-1}) estimated by the three end-member mixing model in the study area.

$$FRa_{dif} = \frac{P\sqrt{D \times \lambda}}{K_d} \times A \quad (16)$$

where P is the production rate, depending on the activity of parent-Th; D is the molecular diffusion coefficient; λ is the decay constant of the isotope, and K_d is the distribution coefficient for the partitioning of Ra between the particulate and dissolved phase, which was assumed to be 80 in seawater (Rama and Moore, 1996); and A is the surface area of the bottom of the ECS that contributes to the diffusion from bottom sediments, which was 2.88×10^5 km^2 in the inner shelf and 4.40×10^5 km^2 in the outer shelf based on the sampling locations. For porosity values between 0.53 and 0.73, the average ^{230}Th and ^{232}Th activities in bottom sediments in the continental shelf of the ECS was reported to be approximately 1.83 dpm cm^{-3} and 2.77 dpm cm^{-3}, respectively (Wang et al., 2006; Du et al., 2010). The diffusivity of dissolved Ra in sediment (D_s) is lower than its molecular diffusivity in seawater ($D_m = 6.9 \times 10^{-5}$ m^2 d^{-1}, Li and Gregory, 1974) and for average porosity value, it is estimated to be 4.1×10^{-5} m^2 d^{-1}. Thus, the maximum diffusive fluxes of ^{226}Ra and ^{228}Ra from the bottom sediments were estimated to be 4.46×10^{13} and 1.13×10^{15} dpm yr^{-1} in the ECS, which correspond to 1.58×10^{-5} dpm cm^{-2} d^{-1} and 4.02×10^{-4} dpm cm^{-2} d^{-1}, respectively. This was on the same order of magnitude as in the Mississippi discharge zone (Krest et al., 1999) but much smaller than the diffusive fluxes in the Bamen Bay with mangroves (Gu, 2015). This implies that the diffusive flux from the bottom sediments could differ depending on the types of the sediment.

4.3.2. The estimation of SGD flux

Since the half-life of ^{226}Ra is much longer than the water residence time in the study area, the amount of ^{226}Ra loss from radioactive decay could be ignored. To estimate the SGD flux, the amount of ^{226}Ra derived from SGD into the study area was necessary, which could be obtained by subtracting diffusional flux from sediments from the total excess ^{226}Ra flux. The total excess ^{226}Ra flux, calculated by dividing the total inventory of excess ^{226}Ra by the residence time discussed above, is estimated to be 5.36×10^{14} dpm yr^{-1}. Similarly, the excess ^{226}Ra flux in the inner shelf water is estimated to be 2.30×10^{12} dpm d^{-1}. That is, the excess Ra flux in the inner shelf was much higher than the outer shelf although it has larger surface area and volume of water. These results showed a strong terrestrial input. Then, as is described above, the amount of ^{226}Ra derived from SGD into the study area is estimated to be approximately 4.91×10^{14} dpm yr^{-1}, after subtracting maximum diffusive flux from the bottom sediments discussed above. This ^{226}Ra flux from SGD can be converted to total groundwater flux by dividing ^{226}Ra concentration in local groundwater ($^{226}Ra_{gw}$, dpm 100 L^{-1}).

$$SGD = \frac{F^{226}Ra_{SGD}}{^{226}Ra_{gw}} \quad (17)$$

In order to have excess Ra to the system, the ^{226}Ra end-member of SGD must be have higher activity than that of the surface water in nearshore stations and should have a similar or even higher (^{228}Ra/^{226}Ra) AR as that of the excess radium in the seawater. As is shown in Fig. 7, the (^{228}Ra/^{226}Ra) AR in the groundwater samples (excluding the values lower than the seawater) has a slope of around 6.59. The excess (^{228}Ra/^{226}Ra).AR in the seawater samples shows a consistent result around 5.07. Therefore, the groundwater samples could be the proper SGD end-member. The activities of ^{226}Ra in the groundwater samples ranged from 29.4 to 90.5 dpm 100 L^{-1}. To estimate the minimum SGD flux, the highest activity of ^{226}Ra in the groundwater samples was used, which is 90.5 ± 2.3 dpm 100 L^{-1}. Dividing the SGD derived ^{226}Ra flux by this ^{226}Ra activity in the groundwater, yields the SGD fluxes into the ECS of $(5.42 \pm 0.14) \times 10^{11}$ m^3 yr^{-1}, which is (47 ± 1) % of the total riverine discharge along the coast into the ECS (approximately 1.14×10^{12} m^3 yr^{-1} according to the Changjiang River Sediment Bulletin recorded at the Datong Station and the proportion of the Changjiang River discharge of the total river discharge along the coast of the ECS, based on the list given in Liu et al. (2009)). The estimated SGD into the ECS included not only the fresh groundwater discharge but also the recirculated seawater discharge. Compared to the Gu et al. (2012) reported in the Changjiang River effluent plume, this value is a lower estimate. A higher SGD rate was also reported in the Yellow River estuary, the second largest river emptying into the Bohai Sea of China (Xu et al., 2014; Xia et al., 2016), which indicated that large river discharge tends to lead to more intense SGD within the estuaries. This is because they include discharge that occurs beyond the shoreline, and includes the inner shelf (Moore, 2010). Table 5 shows a comparison of SGD fluxes using Ra isotopes around the world. Our SGD flux estimate is well within the range of global estimates, although geomorphological differences do exist among the various locations.

4.4. Evaluation of SGD-derived nutrient fluxes to the ECS

The spatial and temporal distribution of nutrient in the ECS has been reported in several earlier studies (Wang et al., 2002; Gao et al., 2004; Zhang et al., 2007a; Chen, 2008; Pei et al., 2009; Mi et al., 2012). The sources and transport of nutrient in the ECS, including riverine input, deposition from the atmosphere, exchange between sediment and overlying seawater, export to the open sea, have also been reported (Chen et al., 1995; Chen, 1996; Liu et al., 2000; Guo et al., 2006; Zhang et al., 2007a; Gao et al., 2008; Fu et al., 2008; Liu et al., 2009; Yu et al., 2012; Dong et al., 2016). However, the report on the contribution of

Table 4
The non-conservative ^{226}Ra and ^{228}Ra fluxes used in the estimation of the SGD flux in the inner and outer shelf zones of the ECS.

Region	Tracer	I ($\times 10^{13}$ dpm)	τ	FRa_{ex}	F_{dif}	FRa_{SGD}	SGD	Total River
Inner shelf	^{226}Ra	7.3	31.7 ± 14.5 d	0.69 × 10^{14} dpm month^{-1}	0.051 × 10^{13} dpm month^{-1}	0.70 × 10^{14} dpm month^{-1}	0.77 × 10^{11} m^3 month^{-1}	1.14 × 10^{12} m^3 a^{-1}
	^{228}Ra	45.3		4.35 × 10^{14} dpm month^{-1}	1.28 × 10^{13} dpm month^{-1}	4.23 × 10^{14} dpm month^{-1}	0.92 × 10^{11} m^3 month^{-1}	
Outer shelf	^{226}Ra	62.5	1.53 ± 0.75 a	4.08 × 10^{14} dpm a^{-1}	3.85 × 10^{13} dpm a^{-1}	3.69 × 10^{14} dpm a^{-1}	4.08 × 10^{11} m^3 a^{-1}	
	^{228}Ra	350		22.9 × 10^{14} dpm a^{-1}	97.6 × 10^{13} dpm a^{-1}	13.1 × 10^{14} dpm a^{-1}	2.86 × 10^{11} m^3 a^{-1}	
Whole continental shelf	^{226}Ra	69.8	1.30 ± 0.27 a	5.36 × 10^{14} dpm a^{-1}	4.46 × 10^{13} dpm a^{-1}	4.91 × 10^{14} dpm a^{-1}	5.42 × 10^{11} m^3 a^{-1}	
	^{228}Ra	395		30.4 × 10^{14} dpm a^{-1}	113 × 10^{13} dpm a^{-1}	19.1 × 10^{14} dpm a^{-1}	4.17 × 10^{11} m^3 a^{-1}	
Total SGD/River							36%–47%	

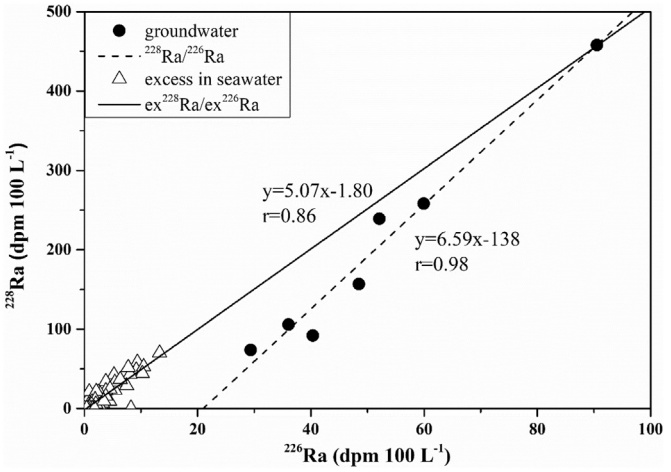

Fig. 7. Plots of excess ^{228}Ra versus excess ^{226}Ra in the seawater of the ECS and ^{228}Ra versus ^{226}Ra in the groundwater samples along the coast of the ECS. The lines indicate the correlation between the two Ra isotopes. Solid line shows the slope of the excess ^{228}Ra versus excess ^{226}Ra for seawater samples; dash lines show the slope of the ^{228}Ra versus ^{226}Ra for groundwater samples.

SGD to the nutrient in the ECS was limited to the Xiangshan Bay, which is near the coast of Zhejiang Province (Wu et al., 2013). Therefore, we use the SGD into the ECS discussed above and the nutrient concentration in the groundwater along the coast to estimate the SGD-derived nutrient fluxes into the ECS. The nutrient concentration in the groundwater samples showed obvious seasonal variations. The average concentrations of DIN, DIP and DSi were 186 ± 3.1, 1.44 ± 1.39 and 277 ± 2.3 (n = 25) μmol L^{-1}, respectively, in spring (March 2012); the average concentrations in summer (July to August 2012) were 135 ± 79.5, 3.30 ± 1.98 and 293 ± 73.7 (n = 23) μmol L^{-1} for DIN, DIP and DSi, respectively. The ratios of Si/N and N/P in the groundwater were both higher than the Redfield ratio. The average ratios of Si/N and N/P were 2.18 and 40.8, respectively, in summer.

The distribution of dissolved inorganic nutrient in the ECS showed that the high values appeared in the Changjiang River estuary and the nearshore area in summer 2013 (Dong, 2015). The nutrient concentration was lower in the surface water during summer compared to spring, but higher in the bottom water. This was mainly due to a large number of terrestrial inputs and nutrient consumption by the phytoplankton above the eutrophic layer. For the terrestrial input, we should not only pay attention to the riverine input but also SGD-derived nutrient input into the ECS. In order to estimate SGD-derived nutrient fluxes to the ECS, we multiplied the average groundwater end-member concentration of nutrient by the estimated SGD-water flux. The SGD-derived DIN, DIP and DSi fluxes into the study area in ECS is estimated to be (7.32 ± 0.19) × 10^{10}, (1.79 ± 0.05) × 10^{9} and (1.59 ± 0.04) × 10^{11} mol yr^{-1}, respectively. The nutrient inputs through the river water were determined by multiplying the river discharge by the concentrations of the nutrient in river water, which was estimated to be 8.56 × 10^{10}, 0.73 × 10^{9} and 1.14 × 10^{11} mol yr^{-1} for DIN, DIP and DSi, respectively. These calculations demonstrated that the SGD input of DIN, DIP and DSi into the ECS was comparable to the river inputs which cannot be ignored.

It is well known that N and P enrichment may lead to deficiency of dissolved silicate, hence, limit the diatom growth, and result in food web changes in aquatic system (Conley et al., 1993; Liu et al., 2009). In August 2013, the ratio of Si/N in the coastal surface water of the ECS was lower than the Redfield ratio, while the ratio of N/P was much higher than the Redfiled ratio. However, in the case of southern and eastern area of the ECS, the ratio of Si/N was higher than the Redfield ratio, and the ratio of N/P approached the Redfield ratio (Dong, 2015). Thus, the SGD derived nutrient fluxes with higher silicate than nitrogen

Table 5
A comparison of SGD rate in some large scale study areas around the world by using biogeochemical tracers.

Study area	Tracer	SGD rate/dm^3 cm^{-2} d^{-1}	Reference
Northeast Gulf of Mexico	Radon	$(2-10)\times10^{-3}$	Cable et al., 1996
Gulf of Lion	^{226}Ra ^{228}Ra	$(2.5–9.5)\times10^{-5}$	Ollivier et al., 2008
Baltic sea, Germany	^{222}Rn	3.6×10^{-2}	Purkl and Eisenhauer, 2004
Mediterranean, Balearic Islands	^{223,224,226,228}Ra	$(1.16–1.86)\times10^{-5}$	Rodellas et al., 2014
Mediterranean Sea	228Ra	$(0.2–3.0)\times10^{-3}$	Rodellas et al., 2015
Yellow Sea, China	^{226}Ra, ^{228}Ra	2.74×10^{-4}	Kim et al., 2005
	^{228}Ra	1.15×10^{-3}	Liu et al., 2017
Northern South China Sea, China	^{223,224,226,228}Ra	$(0.75–1.46)\times10^{-4}$	Liu et al., 2012
upper Atlantic Ocean	^{228}Ra	$(0.58–1.1)\times10^{-3}$	Moore et al., 2008
Atlantic and Indo-Pacific Oceans between 60°S and 70°N	^{228}Ra	$(2.2\pm0.5)\times10^{-3}$	Kwon et al., 2014
East China Sea, China	^{223,224,226,228}Ra	$(3.9\pm0.1)\times10^{-4}$	This study

as well as more nitrogen than phosphorus may lead to potential phosphorus limitation for phytoplankton production in the ECS. It has been reported that when P was deficient and N was over-load, the dominant species of phytoplankton communities readily changed from diatoms to dinoflagellates (Richardson, 1997). Therefore, we suggest that the nutrient input by SGD may have an important impact on the coastal ecosystem of the ECS. In the ECS, frequent harmful algal blooms (*Prorocentrum dentatum and Karenia mikimokoi*) have occurred in coastal waters of the ECS (Zhu et al., 1997; Li et al., 2007). Meanwhile, it was reported that blooms dominated by diatoms have decreased, but non-diatom species dominated blooms have increased (Li et al., 2007). The frequency of occurrence of the hypoxia events off the Changjiang River Estuary has been documented (Li et al., 2002; Zhu et al., 2011, 2017; Chen et al., 2007). Although there is no direct evidence that SGD can influence the formation and sustenance of harmful blooms and other environmental problems, SGD does play an important role in all these eco-environmental problems in the ECS which need to be studied further.

5. Summary

In this investigation, we have utilized Ra isotopes to estimate the SGD flux into the continental shelf of the ECS. Three end-member mixing model (temperature, salinity and ^{226}Ra) and the mass balance model were used to estimate the amount of conservative and non-conservative components of radium for SGD and the associated nutrient fluxes in the ECS. We draw the following conclusions:

1) A short residence time was estimated in the inner shelf (31.7 ± 14.6 days), indicating a more dynamic region along the coastline compared to that of the whole continental shelf (1.30 ± 0.27 years).
2) The amount of SGD including the fresh groundwater discharge and the recirculated seawater discharge is estimated to be $(5.42\pm0.14)\times10^{11}$ m^3 yr^{-1}, which is 47 ± 1% of the total river discharge along the coast of ECS.
3) The SGD-derived nutrient fluxes were estimated to be about 0.7 (DIN), 2.2 (DIP) and 1.4 (DSi) times the corresponding riverine inputs. Furthermore, the SGD-driven nutrient had obviously high DIN/DIP ratios, which could impact the structure of the ecosystem of the ECS, especially in the estuary and coastal areas.
4) Even though there is a large riverine input from the Changjiang River, the SGD is another important source of nutrient to the ECS, which may play an important role for eutrophication resulting in the formation and sustenance of red tides and hypoxia in the ECS.

Acknowledgements

This work was supported by the funds of Chinese Ministry of Science and Technology (Nos. 2016YFA0600904; 2011CB409801).

References

Aller, R., 1998. Mobile deltaic and continental shelf muds as suboxic, fluidized bed reactors. Mar. Chem. 61 (3), 143–155.
Beardsley, R., Limeburner, R., Yu, H., Cannon, G., 1985. Discharge of the Changjiang (Yangtze River) into the East China Sea. Cont. Shelf Res. 4, 57–76.
Bianchi, T., Allison, M., 2009. Large-river delta-front estuaries as natural "recorders" of global environmental change. Proc. Natl. Acad. Sci. 106 (20), 8085–8092.
Burdige, D., 2007. Preservation of organic matter in marine sediments: controls, mechanisms, and an imbalance in sediment organic carbon budgets? Chem. Rev. 107 (2), 467–485.
Cable, J., Burnett, W., Chanton, J., Weatherly, G., 1996. Estimating groundwater discharge into the northeastern Gulf of Mexico using radon-222. Earth Planet. Sci. Lett. 144 (3), 591–604.
Chang, P., Isobe, A., 2003. A numerical study on the Changjiang diluted water in the Yellow and East China Seas. J. Geophys. Res.: Oceans (C9), 108.
Chen, C., 1996. The Kuroshio intermediate water is the major source of nutrients on the East China Sea continental shelf. Oceanol. Acta 19 (5), 523–527.
Chen, C., 2008. Distributions of nutrients in the East China Sea and the South China Sea connection. J. Oceanogr. 64 (5), 737–751.
Chen, C., Ruo, R., Paid, S., Liu, C., Wong, G., 1995. Exchange of water masses between the East China Sea and the Kuroshio off northeastern Taiwan. Cont. Shelf Res. 15 (1), 19–39.
Chen, C., Gong, G., Shiah, F., 2007. Hypoxia in the East China Sea: one of the largest coastal low-oxygen areas in the world. Mar. Environ. Res. 64 (4), 399–408.
Cochran, J., 1992. The oceanic chemistry of uranium and thorium series nuclides [M]. In: Uranium-Series Disequilibrium: Applications to Earth, Marine and Environmental Sciences. Oxford Science Publications Clarendon Press, pp. 334–395.
Conley, D., Schelske, C., Stoermer, E., 1993. Modification of the biogeochemical cycle of silica with eutrophication. Mar. Ecol. Prog. Ser. 101 (1–2), 179–192.
Dong, S., 2015. Distributions and Variations and Cross Shelf Exchange of Nutrients in the East China Sea. Ocean University of China, Qingdao, Shandong, China (in Chinese with English abstract).
Dong, S., Liu, S., Ren, J., Li, J., Zhang, J., 2016. Preliminary estimates of cross shelf transport flux of nutrients in the East China Sea in spring (in Chinese with English abstract). Mar. Environ. Sci. 35 (3), 385–391.
Du, J., Wu, Y., Huang, D., Zhang, J., 2010. Use of ^{7}Be, ^{210}Pb and ^{137}Cs tracers to the transport of surface sediments of the Changjiang River Estuary, China. J. Mar. Syst. 82, 286–294.
Feng, S., Li, F., Li, S., 1999. An Introduction to Marine Science. Higher Education Press, Beijing, China, pp. 470–482.
Fu, M., Zhao, W., Wang, J., Miao, H., 2008. Contribution of atmospheric wet deposition to nutrients in the Yangtze estuary. Environ. Sci. 29 (10), 2703–2709.
Gao, S., Lin, Y., Jin, M., Gao, D., 2004. Distribution features of nutrients and nutrient structure in the East China Sea and the Yellow Sea in spring and autumn (in Chinese with English abstract). Donghai Mar. Sci. 22 (4), 38–50.
Gao, L., Li, D., Ding, P., 2008. Nutrient budgets averaged over tidal cycles off the Changjiang (Yangtze River) Estuary. Estuar. Coast. Shelf Sci. 77 (3), 331–336.
Gonneea, M., Morris, P., Dulaiova, H., Charette, M., 2008. New perspectives on radium behavior within a subterranean estuary. Mar. Chem. 109, 250–267.
Gu, H., 2015. A Quantitative Study on the Sources and Sinks of Radium Isotopes in near-Shore Waters-Taking Changjiang Estuary and its Adjacent Offshore Area, Bamen Lagoon, Gaolong Bay and Boao Bay in Hainan for Example. East China Normal University, Shanghai, China (in Chinese with English abstract).
Gu, H., Moore, W., Zhang, L., Du, J., Zhang, J., 2012. Using radium isotopes to estimate the residence time and the contribution of submarine groundwater discharge (SGD) in the Changjiang River effluent plume, East China Sea. Cont. Shelf Res. 35, 95–107.
Guo, X., Miyazawa, Y., Yamagata, T., 2006. The Kuroshio onshore intrusion along the shelf break of the East China Sea: the origin of the Tsushima warm current. J. Phys. Oceanogr. 36 (12), 2205–2231.
Hedges, J., Keil, R., 1995. Sedimentary organic matter preservation: an assessment and speculative synthesis. Mar. Chem. 49 (2), 81–115.
Ji, T., Du, J., Moore, W., Zhang, G., Su, N., Zhang, J., 2013. Nutrient inputs to a Lagoon through submarine groundwater discharge: the case of Laoye Lagoon, Hainan, China. J. Mar. Syst. 111-112, 253–262.
Kim, G., Ryu, J., Yang, H., Yun, S., 2005. Submarine groundwater discharge (SGD) into

the Yellow Sea revealed by ^{228}Ra and ^{226}Ra isotopes: implications for global silicate fluxes. Earth Planet. Sci. Lett. 237, 156–166.
Krest, J., Harvey, J., 2003. Using natural distributions of short-lived radium isotopes to quantify groundwater discharge and recharge. Limnol. Oceanogr. 48, 290–298.
Krest, J., Moore, W., Rama, 1999. ^{226}Ra and ^{228}Ra in the mixing zones of the Mississippi and Atchafalaya rivers: indicators of groundwater input. Mar. Chem. 64, 129–152.
Kwon, E., Kim, G., Primeau, F., Moore, W., Cho, H., DeVries, T., Sarmiento, J., Charette, M., Cho, Y., 2014. Global estimate of submarine groundwater discharge based on an observationally constrained radium isotope model. Geophys. Res. Lett. 41 (23), 8438–8444.
Lee, H., Chao, S., 2003. A climatological description of circulation in and around the East China Sea. Deep-Sea Res. II 50, 1065–1084.
Li, Y., 1995. Material exchange between the East China Sea and the Kuroshio current. Terr. Atmos. Ocean. Sci. 5 (4), 625–631.
Li, Y., Gregory, S., 1974. Diffusion of ions in sea water and in deep-sea sediments. Geochim. Cosmochim. Acta 38 (5), 703–714.
Li, D., Zhang, J., Huang, D., Wu, Y., Liang, J., 2002. Oxygen depletion off the Changjiang (Yangtze River) estuary. Sci. China. Ser. D Earth Sci. 45 (12), 1137–1146.
Li, M., Xu, K., Watanabe, M., Chen, Z., 2007. Long-term variations in dissolved silicate, nitrogen, and phosphorus flux from the Yangtze River into the East China Sea and impacts on estuarine ecosystem. Estuar. Coast. Shelf Sci. 71, 3–12.
Liu, S., Zhang, J., Chen, H., 2000. Chemical oceanography of bioactive elements in the Yellow Sea and the East China Sea (in Chinese with English abstract). Mar. Environ. Sci. 19 (1), 68–74.
Liu, S., Zhang, J., Chen, H., Zhang, G., 2005. Factors influencing nutrient dynamics in the eutrophic Jiaozhou Bay, North China. Prog. Oceanogr. 66, 66–85.
Liu, S., Hong, G., Zhang, J., Ye, X., Jiang, X., 2009. Nutrient budgets for large Chinese estuaries. Biogeosciences 6, 2245–2263.
Liu, Q., Dai, M., Chen, W., Huh, C., Wang, G., Li, Q., Charette, M., 2012. How significant is submarine groundwater discharge and its associated dissolved inorganic carbon in a river-dominated shelf system? Biogeosciences 9, 1777–1795.
Liu, J., Su, N., Wang, X., Du, J., 2017. Submarine groundwater discharge and associated nutrient fluxes into the Southern Yellow Sea: a case study for semi-enclosed and oligotrophic seas-implication for green tide bloom. J. Geophys. Res.: Oceans 122 (1), 139–152.
Mao, H., Ren, Y., Wan, G., 1964. A preliminary investigation on the application of using T-S diagrams for the quantitative analysis of the water masses in the shallow water area. Oceanol. Limnol. Sin. 6, 1–22.
McKee, B., Aller, R., Allison, M., Bianchi, T., Kineke, G., 2004. Transport and transformation of dissolved and particulate materials on continental margins influenced by major rivers: benthic boundary layer and seabed processes. Cont. Shelf Res. 24 (7), 899–926.
Meade, R., 1996. River-sediment inputs to major deltas [M]. In: Sea-level Rise and Coastal Subsidence. Springer Netherlands, pp. 63–85.
Mi, T., Yao, Q., Meng, J., Zhang, X., Liu, S., 2012. Distributions of nutrients in the southern Yellow Sea and East China Sea in spring and summer 2011 (in Chinese with English abstract). Oceanol. Limnol. Sin. 43 (3), 678–688.
Moore, W., 1996. Large groundwater inputs to coastal waters revealed by ^{226}Ra enrichments. Nature 380 (6575), 612–614.
Moore, W., 2010. The effect of submarine groundwater discharge on the ocean. Annu. Rev. Mar. Sci. 2, 59–88.
Moore, W., Amold, R., 1996. Measurement of ^{223}Ra and ^{224}Ra in coastal waters using a delayed coincidence counter. J. Geophys. Res. 101, 1321–1329.
Moore, W., Sarmiento, J., Key, R., 2008. Submarine groundwater discharge revealed by ^{228}Ra distribution in the upper Atlantic Ocean. Nat. Geosci. 1 (5), 309–311.
Nozaki, Y., Kasemsupaya, V., Tsubota, H., 1989. Mean residence time of the shelf water in the East China and the yellow seas determined by ^{228}Ra/^{226}Ra measurements. Geophys. Res. Lett. 16 (11), 1297–1300.
Nozaki, Y., Tsubota, H., Kasemsupaya, V., Yashima, M., Ikuta, N., 1991. Residence times of surface water and particle-reactive ^{210}Pb and ^{210}Po in the East China and yellow seas. Geochim. Cosmochim. Acta 55, 1265–1272.
Ollivier, P., Claude, C., Radakovitch, O., Hamelin, B., 2008. TIMS measurements of ^{226}Ra and ^{228}Ra in the Gulf of Lion, an attempt to quantify submarine groundwater discharge. Mar. Chem. 109 (3), 337–354.
Pei, S., Shen, Z., Laws, E., 2009. Nutrient dynamics in the upwelling area of Changjiang (Yangtze River) Estuary. J. Coast. Res. 569–580.
Purkl, S., Eisenhauer, A., 2004. Determination of radium isotopes and ^{222}Rn in a groundwater affected coastal area of the Baltic Sea and the underlying sub-sea floor aquifer. Mar. Chem. 87 (3), 137–149.
Rama, Moore, W., 1996. Using the radium quartet for evaluating groundwater input and water exchange in salt marshes. Geochim. Cosmochim. Acta 60 (23), 4645–4652.
Richardson, K., 1997. Harmful or exceptional phytoplankton blooms in the marine ecosystem. Adv. Mar. Biol. 31, 301–385.
Rodellas, V., Garcia-Orellana, J., Tovar-Sánchez, A., Basterretxea, G., López-Garcia, J.M., Sánchez-Quiles, D., Garcia-Solsona, E., Masqué, P., 2014. Submarine groundwater discharge as a source of nutrients and trace metals in a Mediterranean bay (Palma Beach, Balearic Islands). Mar. Chem. 160, 56–66.
Rodellas, V., Garcia-Orellana, J., Masqué, P., Feldman, M., Weinstein, Y., 2015. Submarine groundwater discharge as a major source of nutrients to the Mediterranean Sea. Proc. Natl. Acad. Sci. 112 (13), 3926–3930.
Santos, I., Burnett, W., Chanton, J., Mwashote, B., Suryaputra, I., Dittmar, T., 2008. Nutrient biogeochemistry in a Gulf of Mexico subterranean estuary and groundwater-derived fluxes to the coastal ocean. Limnol. Oceanogr. Methods 53 (2), 705–718.
Santos, I., Burnett, W., Dittmar, T., Suryaputra, I., Chanton, J., 2009. Tidal pumping drives nutrient and dissolved organic matter dynamics in a Gulf of Mexico subterranean estuary. Geochim. Cosmochim. Acta 73, 1325–1339.
Su, J., 1998. Circulation dynamics of the China Seas north of 18°N. In: Robinson, A.R., Brink, K.H. (Eds.), The Sea. vol. 11. John Wiley & Sons Inc, New York, pp. 483–505.
Su, N., Du, J., Moore, W.S., Liu, S., Zhang, J., 2011. An examination of groundwater discharge and the associated nutrient fluxes into the estuaries of eastern Hainan Island, China using ^{226}Ra. Sci. Total Environ. 409 (19), 3909–3918.
Su, N., Du, J., Duan, Z., Deng, B., Zhang, J., 2015. Radium isotopes and their environmental implications in the Changjiang River system. Estuar. Coast. Shelf Sci. 156, 155–164.
Takano, K., 1991. Oceanography of Asian Marginal Seas. In: Elsevier Oceanography Series, pp. 1–431.
Tsunogai, S., Watanabe, S., Nakamura, J., Ono, T., Sato, T., 1997. A preliminary study of carbon system in the East China Sea. J. Oceanogr. 53 (1), 9–17.
Wang, B., Shan, B., Zhan, R., Zang, J., 2002. Budget model of inorganic nitrogen in the Bohai and Yellow Sea (in Chinese with English abstract). Mar. Sci. 26 (2), 33–36.
Wang, Z., Liu, C., Zhu, Z., Masatoshi, Y., 2006. Precipitation of authigenic uranium and its controlling mechanism in sediments from the East China Sea and Okinawa Trough (in Chinese with English abstract). Geochimica 35 (3), 240–248.
Wang, X., Du, J., Ji, T., Wen, T., Liu, S., Zhang, J., 2014. An estimation of nutrient fluxes via submarine groundwater discharge into the Sanggou Bay-a typical multi-species culture ecosystem in China. Mar. Chem. 167, 113–122.
Wang, X., Yu, Z., Fan, W., Song, X., Cao, X., Yuan, Y., 2015. Nutrient fluxes in the Changjiang River estuary and adjacent waters-a modified box model approach. Chin. J. Oceanol. Limnol. 33, 176–193.
Webster, I., Hancock, G., Murray, A., 1995. Modeling the effect of salinity on radium desorption from sediments. Geochim. Cosmochim. Acta 59, 2469–2476.
Wu, H., 2015. Cross-shelf penetrating fronts: a response of buoyant coastal water to ambient pycnocline undulation. J. Geophys. Res.: Oceans 120 (7), 5101–5119.
Wu, H., Zhu, J., Shen, J., Wang, H., 2011. Tidal modulation on the Changjiang River plume in summer. J. Geophys. Res.: Oceans (C8), 116.
Wu, Z., Zhou, H., Zhang, S., Liu, Y., 2013. Using ^{222}Rn to estimate submarine groundwater discharge (SGD) and the associated nutrient fluxes into Xiangshan Bay, East China Sea. Mar. Pollut. Bull. 73 (1), 183–191.
Wu, H., Shen, J., Zhu, J., Zhang, J., Li, L., 2014. Characteristics of the Changjiang plume and its extension along the Jiangsu Coast. Cont. Shelf Res. 76, 102–123.
Xia, D., Yu, Z., Xu, B., Gao, M., Mi, T., Jiang, X., Yao, P., 2016. Variations of hydrodynamics and submarine groundwater discharge in the Yellow River estuary under the influence of the water-sediment regulation scheme. Estuar. Coasts 39 (2), 333–343.
Xu, B., Xia, D., Burnett, W.C., Dimova, N.T., Wang, H., Zhang, L., Gao, M., Jiang, X., Yu, Z., 2014. Natural ^{222}Rn and ^{220}Rn indicate the impact of the Water–Sediment Regulation Scheme (WSRS) on submarine groundwater discharge in the Yellow River estuary, China. Appl. Geochem. 51, 79–85.
Yanagi, T., 1994. Material transport in the Yellow/East China Seas. Engan Kaiyo Kenkyu Noto 31, 239–256.
Yu, Y., Song, J., Li, X., Yuan, H., Li, N., 2012. Distribution, sources and budgets of particulate phosphorus and nitrogen in the East China Sea. Cont. Shelf Res. 43, 142–155.
Yuan, D., Hsueh, Y., 2010. Dynamics of the cross-shelf circulation in the Yellow and East China Seas in winter. Deep-Sea Res. II 57 (19), 1745–1761.
Zeng, D., Ni, X., Huang, D., 2012. Temporal and spatial variability of the ZheMin Coastal Current and the Taiwan Warm Current in winter in the southern Zhejiang coastal sea (in Chinese). Sci. Sin. Terrae 42 (7), 1123–1134.
Zhang, J., Liu, S., Ren, J., Wu, Y., Zhang, G., 2007a. Nutrient gradients from the eutrophic Changjiang (Yangtze River) Estuary to the oligotrophic Kuroshio waters and re-evaluation of budgets for the East China Sea Shelf. Prog. Oceanogr. 74 (4), 449–478.
Zhang, L., Liu, Z., Zhang, J., Hong, G., Park, Y., Zhang, H., 2007b. Reevaluation of mixing among multiple water masses in the shelf: an example from the East China Sea. Cont. Shelf Res. 27 (15), 1969–1979.
Zhu, M., Li, R., Mu, X., Ji, R., 1997. Harmful algal blooms in China seas. Ocean Polar Res. 19 (2), 173–184.
Zhu, Z., Zhang, J., Wu, Y., Zhang, Y., Lin, J., Liu, S., 2011. Hypoxia off the Changjiang (Yangtze River) Estuary: oxygen depletion and organic matter decomposition. Mar. Chem. 125 (1), 108–116.
Zhu, Z., Wu, H., Liu, S., Wu, H., Huang, D., Zhang, J., Zhang, G., 2017. Hypoxia off the Changjiang (Yangtze River) estuary and in the adjacent East China Sea: quantitative approaches to estimating the tidal impact and nutrient regeneration. Mar. Pollut. Bull. 125 (1–2), 103–114.